(Received 11 November 2024, Accepted 10 January 2025, Scheduled 20 January 2025)

A Unified Approach for the Design and Analysis of Fabry-Perot Antennas with Nonuniform PRS

Akshar Tripathi[1] and Mahesh P. Abegaonkar[2,*]

[1]Department of Electrical Engineering, Indian Institute of Technolgy Delhi, India
[2]Centre for Applied Research in Electronics (CARE), Indian Institute of Technology (IIT) Delhi, New Delhi 110016, India

ABSTRACT: In this paper, a ray-tracing based mathematical model is proposed for the analysis and design of Fabry-Perot antennas with a nonuniform Partially Reflective Surface (PRS). The use of nonuniform PRS in FPA's has recently gained attention due to its immense applications such as directivity enhancement and beam-steering. A spatially varying phase profile of the PRS is achieved by the arrangement of various distinct unit cells throughout the surface. The PRS phase and magnitude variation enables the alteration of wavefronts to achieve beam steering along a desired polar and azimuth angle (θ, ϕ). Thus, a simple, robust, and computationally efficient model to find the optimal FPA parameters and phase profiles for beam-steering has been developed in this paper. FPAs were designed using a square PRS for 1-D and 2-D beam steering with a directivity of up to 17 dBi. The model has been verified with the simulated results at 8 GHz and 8.5 GHz, demonstrating consistent field patterns with the full-wave simulations.

1. INTRODUCTION

A high-gain Fabry-Perot Antenna (FPA) consists of a ground plane with a patch antenna and a partially reflective surface (PRS) parallel to it. The antenna's remarkable advantages have significantly enhanced the research work in this field. In addition, beam-steering in low-profile FPAs has become increasingly popular due to its wide range of applications in satellite communication and radar technologies.

Beam steering is generally achieved using the concept of phased arrays [1]. Fabry-Perot antennas provides a simple and cost efficient method for beam steering by manipulating the emitted electromagnetic (EM) fields using the PRS phase properties. Beam steering in FPAs has been demonstrated by using nonuniform PRS phase profiles in [2–10]. The use of electronically active metasurfaces to vary the phase profile for beam steering has been investigated in [3, 6–10]. Beam steering has also been achieved mechanically for constructive interference along desired directions [11, 12]. Recent advancements in FPA design involve directivity enhancement using sidelobe suppression [13] and multilayer surfaces [14, 15].

There are currently various methods to analyze Fabry-Perot antennas. A widely used method involves the application of ray tracing in a one-dimensional (1-D) model of the antenna given by [16]. Equivalent circuit models have also been developed [17–19]. In the circuit models, the FPA can be characterised as a transmission line cascaded with lumped elements to model the PRS properties. Additionally, leaky-wave analysis has been used to investigate the magnitude and phase properties of the emitted E-field [20, 21]. Leaky-wave analysis is based on the fact that the surface properties influence the leaky-wave magnitude and phase resulting in different far-field patterns. The ray tracing model given in [16] is applicable only to 1-D FPAs with a constant uniform phase profile. Recent advancements in the ray tracing method involve using the approach to analyze nonuniform PRS along one dimension for antennas with a Flat Top Radiation Pattern (FTRP) [22] and for the analysis of reconfigurable FPAs [23].

The ray tracing model can be further extended to analyze 1-D and 2-D nonuniform PRS structures for FPA design. Therefore, a complete mathematical model of the FPA and PRS using ray tracing is developed and analyzed in this paper. It would provide a simple and efficient method to enhance the design and analysis of antennas with nonuniform PRS profiles. The ray tracing method as developed in [16] would be further extended for a finite nonuniform PRS to obtain a simple mathematical model to analyze any general FPA.

2. FPA MODEL WITH A NONUNIFORM PRS

In the ray tracing method, a 1-D FP model (Fig. 1) is utilized to analyze the phase of each transmitted wave. The maximum radiation at any given angle θ occurs at the resonance condi-

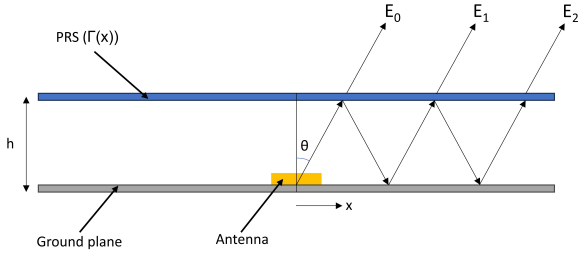

FIGURE 1. Schematic of the 1-D FPA Model.

* Corresponding author: Mahesh Pandurang Abegaonkar (mpjosh@care.iitd.ac.in).

tion, when all the transmitted waves constructively interfere. The base patch antenna can be modelled with a radiation pattern $R(\theta)$. The antenna is placed just above a ground plane with a reflection phase of ψ. A partially reflective surface (PRS) is present at a distance h above the ground plane. For a nonuniform PRS, the reflection coefficient (Γ) and transmission coefficient (T) are functions of x along the PRS. $r(x)$ and $t(x)$ denote the magnitude components, while $\phi(x)$ and $\varphi(x)$ denote the phase components of the reflection and transmission coefficient, respectively.

$$\Gamma(x) = r(x)e^{j\phi(x)} \quad (1)$$

$$T(x) = t(x)e^{j\varphi(x)} \quad (2)$$

For an arbitrary theta, the net electric field viewed from a considerable distance would be the vector sum of all the transmitted rays $E_0, E_1, E_2, \ldots, E_N$.

$$E(\theta) = \sum_{n=0}^{N} E_n \quad (3)$$

The ray E_n consists of a magnitude and a phase component (A_n, Θ_n). Each $E_n = A_n e^{j\Theta_n}$ would be subjected to:

- Phase variations due to path differences and reflections;
- Magnitude variations due to reflection and transmission.

2.1. Magnitude Analysis

After each reflection or transmission, the amplitude will be reduced by a factor of $|\Gamma(x)|$ or $|T(x)|$, respectively. T is the transmission coefficient of the PRS, $E_r R(\theta)$ the electric field provided by the antenna, and β the phase constant of the wave in free space. Let $x_n = (2n+1)h\tan(\theta)$, $r(x_n) = r_n$ and $t(x_n) = t_n$. Hence for $n \geq 1$:

$$A_n = E_r R(\theta)\left(t_{n+1}\prod_{k=1}^{n} r_k\right) \quad (4)$$

2.2. Phase Analysis

After reflection with the ground plane or PRS, the wave will incur a phase change of ψ or $\phi(x)$, respectively. Due to a path difference within the cavity, there is a phase change of $-\beta\frac{2h}{\cos(\theta)}$ between two consecutive transmitted waves. Similarly, there also exists a path difference between two consecutive waves outside the cavity. When we analyze the radiation at an angle theta, wave E_{k-1} has to travel an extra distance of $2h\tan(\theta)\sin(\theta)$ compared to wave E_k to reach the normal plane corresponding to θ. Let $x_n = (2n+1)h\tan(\theta)$, $\phi(x_n) = \phi_n$ and $\varphi(x_n) = \varphi_n$. Setting Θ_0 as the reference, for $n \geq 1$, $\Delta\Theta_n = \Theta_n - \Theta_0$ is given by:

$$\Delta\Theta_n = n\left(-2\beta(h\cos(\theta)) + \psi + \frac{\sum_{k=1}^{n}\phi_k}{n}\right) + (\varphi_{n+1} - \varphi_1) \quad (5)$$

2.3. Net Field at an Arbitrary Angle θ

Using (3), (4), (5) and setting $B_n = A_n e^{j\Theta_0}$, the expression for electric field at an arbitrary angle θ could be written as:

$$E(\theta) = \left(\sum_{n=0}^{N} A_n e^{j\Delta\Theta_n}\right)e^{j\Theta_0} = \left(\sum_{n=0}^{N} B_n e^{j\Delta\Theta_n}\right) \quad (6)$$

Equation (6) can be expressed in matrix form given by:

$$\bar{E}(\theta) = MXP \quad (7)$$

$$\sum_{n=1}^{N}\bar{E}_n = M\underbrace{\begin{bmatrix} 1 & 0 & \cdots & 0 \\ 0 & e^{jK} & \cdots & 0 \\ \vdots & \vdots & \ddots & \vdots \\ 0 & 0 & \cdots & e^{jnK} \end{bmatrix}}_{\text{X = Phase change due to propagation}} P \quad (8)$$

E_i represents the electric field of each ray. $\bar{E}_n$ represents the normalised electric field. All the calculations are done with respect to the phase of E_0. Since the relative phase affects the radiation properties, the phase of E_0 is set to be zero.

$$\bar{E}_n(\theta) = \frac{E_n(\theta)}{E_r R_\theta e^{j\Theta_0}}$$

K is a fixed constant term that depends on the FPA properties which is given by: $K = -2\beta h\cos(\theta) + \psi$.

M represents the magnitude factor of each ray, and P represents the phase change due to the PRS properties.

$$M = \begin{bmatrix} t_1 & t_2 r_1 & \cdots & t_{n+1}(\prod_{k=1}^{n} r_k) \end{bmatrix} \quad (9)$$

$$P = \begin{bmatrix} 1 \\ e^{j(\phi_1+\varphi_2-\varphi_1)} \\ \vdots \\ e^{j(\sum_{k=1}^{n}\phi_k+(\varphi_{n+1}-\varphi_1))} \end{bmatrix} \quad (10)$$

3. ANALYSIS FOR 2-D BEAM STEERING PRS

The above 1-D analysis can be extended to analyze the antenna radiation pattern in two-dimensions (2-D), i.e., the polar and azimuth angles (θ, ϕ). To obtain an estimate of the radiation pattern, the plane that passes through the ground antenna and the desired point on the PRS corresponding to (θ_0, ϕ_0) is chosen. Therefore, the 2-D PRS can be effectively represented by a 1-D model as described in Section 2 along the analysis plane. Fig. 2 represents the plane of analysis. The functions representing the reflection and transmission coefficients will be taken along the intersection line of the analysis plane and the PRS as shown in Fig. 2, and the 2-D base antenna radiation pattern $R(\theta, \phi)$ will be considered in (4) and (5) to calculate the E-field. The axis along the analysis plane is denoted by u.

$$\Gamma(u,\phi)_{2d} = r(u,\phi)e^{j\xi(u,\phi)} \quad (11)$$

$$T(u,\phi)_{2d} = t(u,\phi)e^{j\varphi(u,\phi)} \quad (12)$$

The general matrix form for 2-D field analysis is given as:

$$\bar{E}(\theta,\phi_0) = M_{\theta,\phi_0}X_\theta P_{\theta,\phi_0} \quad (13)$$

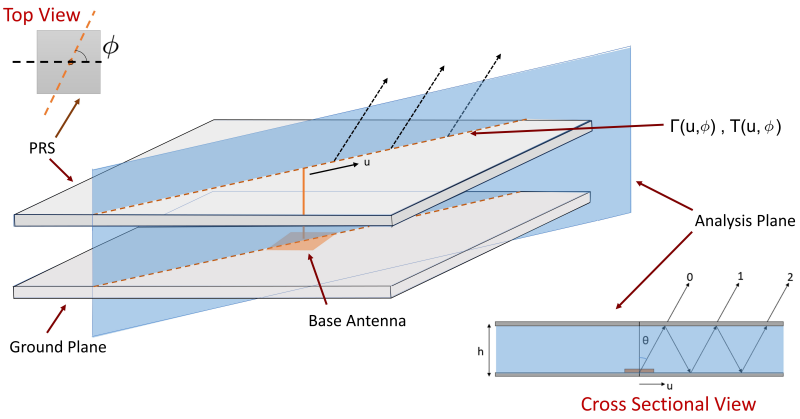

FIGURE 2. Schematic for 2-D analysis of the FPA.

4. PROPOSED METHODS FOR PRS DESIGN AND ANALYSIS

4.1. Phasor Method to Analyze the Radiation Pattern

The sum (6) can be represented in phasor form. For finite PRS structures, the number of E-field rays (N) for computation is a function of theta and the length of the PRS (L).

$$N(\theta) \approx \left\lfloor \frac{L}{2h\tan(\theta)} \right\rfloor \tag{14}$$

In practical FPA designs, the dimensions of the PRS are comparable with $h\tan(\theta)$. By the vector sum for N rays, we can accurately calculate the approximate radiation pattern, beam directivity, and main lobe direction for any nonuniform partially reflective surface. This has been verified with the simulated results given in Section 6. N can be chosen according to the angle of interest for simplifying the computation.

4.2. Beamforming along (θ_0, ϕ_0)

To obtain maximum field intensity at a given angle, the emitted rays, i.e., E_n, must be around the same phase, which would lead to constructive interference of each of the transmitted beams. Since the magnitude of B_n decreases exponentially as n increases, and the source illuminates the central region majorly, the initial field waves would have a major amplitude contribution to the vector sum (6). So to ensure a beam directed at an angle θ_0, the phase difference between two consecutive emitted waves must go to $2m\pi$.

$$\Delta\Theta_n - \Delta\Theta_{n-1} = 2m\pi; \quad m = 0, \pm1, \pm2, \ldots \tag{15}$$

$$-2\beta(h\cos(\theta)) + \psi + (\phi_n) + (\varphi_{n+1} - \varphi_n) = 2m\pi \tag{16}$$

$$\delta_n = K + (\phi_n) + (\varphi_{n+1} - \varphi_n) = 2m\pi \tag{17}$$

K refers to the fixed constant term specified by the FPA design parameters. Thus, a resonance condition is set for the beam from the first reflection point leading to high transmission at the given angle and frequency. The condition (16) gives an accurate value for the height of the cavity to obtain an intense beam at angle θ_0 for any azimuth plane angle. There might be a slight deviation of the main lobe by a few degrees due to the non-significant terms in the vector sum or due to mutual coupling between unit cell elements, which can be further tuned by slightly varying either the height of the cavity or phase balancing a few more terms in (6). Hence by solving the N simultaneous recursive equations in (17), the desired phase profile can be obtained. In addition, the PRS reflection and transmission profiles can be approximately modelled as general functions that are linear in parameters. By substituting the function in terms of its parameters in (17), we can obtain a set of linear equations that can be solved to obtain a functional form of the PRS profile. PRS unit cells could then be designed with approximate reflection and transmission properties such that the waves constructively interfere.

4.3. Nullforming along (θ_0, ϕ_0)

Similar to Section 4.2, a null can be achieved at a specified direction by ensuring that all of the rays destructively interfere with each other, for twhich the vector sum (6) must be made to attain a near zero value using the FPA parameters.

5. PRS DESIGN TO VERIFY THE PROPOSED METHODS

To verify beam steering using the 1-D and 2-D analysis models, a suitable square PRS was designed and simulated at 8 GHz and 8.5 GHz according to the methods proposed in Section 4. Fig. 3(b) represents the used unit cell, which consists of a metallic square patch on one side of a substrate having a relative permittivity of 4.3 and a loss tangent of 0.02. The periodicity of the unit cells in the PRS is 15 mm. The size of the metallic patch was varied to obtain different values of reflection and transmission coefficients, given in Table 1. The base plate consists of a patch antenna at the coordinates $(0, 0)$ along with a completely reflecting ground plane. The patch antenna radiates uniformly in all directions. The simulated $|s_{11}|$ parameters of the base patch antenna is given by Fig. 3(a). The PRS is placed h mm above the patch antenna, which is centrally located above the ground plane. The PRS unit cell arrangement is denoted by the sequence $\{C_{ij}\}_{PRS} = \{c_{i_j}\}_{j=1}^{N}$, where c_{i_j} denotes the jth unit cell, i the size of the metal patch in mm, and N the num-

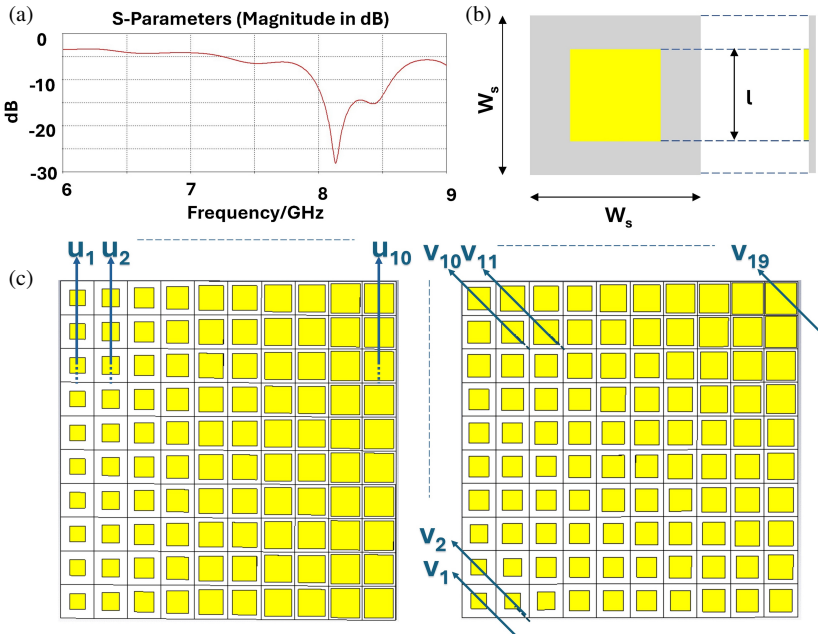

FIGURE 3. (a) Simulated S_{11} of the base antenna. (b) Unit Cell ($W_s = 15$ mm). (c) PRS used for 1-D beam steering (Unit cell sequence: $\{U_{ij}\}_{PRS}$). (d) PRS used for 2-D beam steering (Unit cell sequence: $\{V_{ij}\}_{PRS}$).

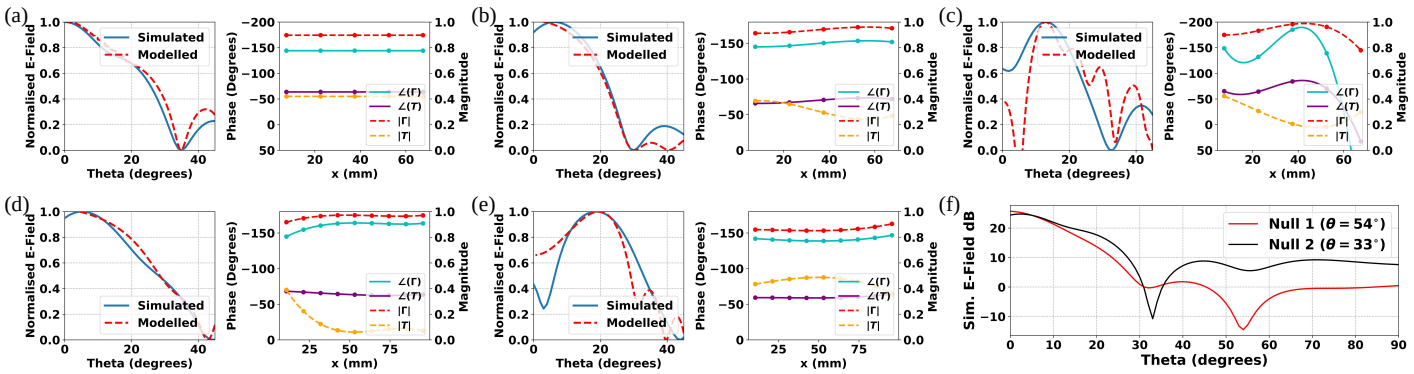

FIGURE 4. Simulated and modelled field results of the FPA designs and plots for the PRS properties along the beam direction (1D: $\{c_{ij}\}_{j=5}^{10}$; 2D: $\{c_{ij}\}_{j=10}^{19}$). Normalised modelled (red) and simulated (blue) Electric-Field results for: (a) PRS_1 ($\theta = 0°$): $\{U_{ij}\}_{PRS_1} = \{c_{11}, c_{11}, c_{11}, c_{11}, c_{11}, c_{11}, c_{11}, c_{11}, c_{11}, c_{11}\}$. (b) PRS_2 ($\theta = 7°$): $\{U_{ij}\}_{PRS_2} = \{c_7, c_7, c_7, c_8, c_9, c_{10}, c_{11}, c_{12}, c_{12}, c_{12}\}$. (c) PRS_3 ($\theta = 13°$): $\{U_{ij}\}_{PRS_3} = \{c_{10}, c_{14}, c_{10}, c_{14}, c_9, c_{11}, c_{12}, c_{13}, c_{13}, c_{14}\}$. (d) PRS_4 ($\theta = 5°$): $\{V_{ij}\}_{PRS_4} = \{c_9, c_9, c_9, c_9, c_{10}, c_9, c_9, c_9, c_{10}, c_{11}, c_{12}, c_{13}, c_{13}, c_{13}, c_{13}, c_{13}, c_{13}, c_{13}, c_{13}\}$. (e) PRS_5 ($\theta = 19°$): $\{V_{ij}\}_{PRS_5} = \{c_{10}, c_{11}, c_{14}, c_9, c_{10}, c_{11}, c_{14}, c_9, c_{10}, c_{11}, c_{14}, c_9, c_{10}, c_{11}, c_{14}, c_9, c_{10}, c_{11}, c_{14}\}$. (f) Simulated E-field results for $\theta_{null} = 54°$ and $33°$: PRS_{null1}: $\{U_{ij}\}_{PRS} = \{c_{11}, c_{11}, c_{11}, c_{11}, c_{11}, c_{11}, c_{11}, c_{11}, c_{11}, c_{11}\}$ and PRS_{null2}: $\{U_{ij}\}_{PRS} = \{c_{11}, c_{11}, c_{11}, c_{11}, c_{11}, c_{11}, c_{13}, c_{11}, c_{13}, c_{11}\}$.

ber of unit cells in the PRS. We use the notation $\{U_{ij}\}_{PRS}$ and $\{V_{ij}\}_{PRS}$ to denote the unit cell sequence of a 1-D and 2-D PRS respectively as depicted in Fig. 3(c) and Fig. 3(d).

5.1. Beams

To achieve a beam at a specified angle, the normal of the equi-phase field plane should be aligned along that direction. The PRS phase profile can be modelled as a generalised function of x with M parameters based on the application (linear, quadratic, sinusoidal, etc.) Hence by solving M simultaneous equations in (17) the desired phase profile can be obtained. To design the surfaces, $\phi(x)$ and $\psi(x)$ are modelled as linear functions, i.e., $\phi(x) = ax + \phi_p$ and $\psi(x) = bx + \psi_p$. Substituting $\phi(x)$ and $\psi(x)$ in (17), a relation for the coefficients of the linear functions is obtained.

$$\delta_n = K + (anp + \phi_p) + (bp) = 2m\pi \tag{18}$$

The periodicity factor of the beam angle is represented by p, which is equal to $2h\tan(\theta)$. Based on the obtained coefficients and initial intercepts ϕ_p and ψ_p, appropriate unit cells were chosen that approximately satisfy the calculated phase profile and computationally maximise the vector sum (6) at θ_{beam}. Using this, three 1-D beamsteering PRS structures, PRS_1, PRS_2, and PRS_3, were designed and analyzed. The PRS properties are given in Figs. 4(a), (b), (c). Similarly following the design

TABLE 1. Unit cell reflection and transmission properties.

Unit Cell	$(\|\Gamma\|, \|T\|)$ (dB)		$(\angle\Gamma\ (^\circ), \angle T\ (^\circ))$	
	8 GHz	8.5 GHz	8 GHz	8.5 GHz
c_9	$(-2.48, -3.8)$	$(-2.2, -4.2)$	$(-129.6, -48.7)$	$(-130.8, -50.9)$
c_{10}	$(-1.58, -5.4)$	$(-1.36, -6.01)$	$(-137.0, -56.4)$	$(-138.2, -58.7)$
c_{11}	$(-0.937, -7.5)$	$(-0.77, -8.4)$	$(-144.2, -63.8)$	$(-145.6, -66.1)$
c_{12}	$(-0.533, -10.3)$	$(-0.41, -11.5)$	$(-150.5, -70.1)$	$(-152.4, -72.3)$
c_{13}	$(-0.256, -14.33)$	$(-0.28, -22.25)$	$(-157.6, -75.77)$	$(-163.2, -63.12)$
c_{14}	$(-2.27, -10.30)$	$(-0.93, -9.02)$	(179.6, 34.14)	$(-147.24, -63.13)$

TABLE 2. Simulated vs modelled beam directions.

PRS Used	Beam Angle (θ, ϕ)		Frequency	Directivity	h (mm)
	Modelled	Simulated			
Fig. 4(a)	(0, 0)	(0, 0)	8 GHz	17 dBi	21.1
Fig. 4(b)	(5, 0)	(7, 0)	8.5 GHz	15.6 dBi	20.1
Fig. 4(c)	(13, 0)	(13, 0)	8 GHz	14 dBi	21
Fig. 4(d)	(4, 45)	(5, 45)	8.5 GHz	11.1 dBi	20.1
Fig. 4(e)	(20, 45)	(19, 45)	8.5 GHz	13.9 dBi	21.1

procedure along the analysis plane of $\phi = 45^\circ$, two 2-D beam-steering antenna designs with different PRS gradients were analyzed with their properties depicted in Figs. 4(d) and (e). Overall, the simulated and modelled FPA main beam directions are summarized in Table 2.

5.2. Nulls

For generating nulls, the aim is to obtain a net zero electric field at the angle θ_{null}. This has been achieved using two design methods. The first method involves using a uniform PRS and finding the optimal height where the net E-field (6) is minimised, i.e., $\frac{dE(h,\theta_{null})}{dh} = 0$ and $\frac{d^2E(h,\theta_{null})}{dh^2} > 0$. PRS_{null1} was designed using this method for a null at 55°. Taking the cavity height ($h = 20.5$ mm) at 8 GHz, a null at 54° is obtained with a null depth of -19.9 dBi. The second method involves altering the PRS profile at a fixed h so that the rays destructively interfere, minimising the phasor sum (6). To obtain a null at 30° and $h = 21$ mm, the first 6 terms of the vector sum is considered. Based on this approach, PRS_{null2} was numerically designed. Simulated results, as given in Fig. 4(f), show that a null is obtained at 33° with a null depth of -18 dBi and a net E-field of -11 dB (V/m).

6. RESULTS AND VERIFICATION

The phasor method as given in Section 4.1 has been used to model the radiation pattern. Fig. 4 demonstrates the simulated and modelled E-field radiation patterns for both 1-D and 2-D FPAs along with the PRS profile. Additionally, the approach to minimise the electric field has also been verified by the simulated data as given in Fig. 4(f). It is observed that the modelled and simulated patterns have a good agreement.

7. CONCLUSION

Using ray-tracing method, we have developed a mathematical model to analyze an FPA with given reflection and transmission profiles in two dimensions (θ, ϕ). The proposed analysis and design technique provides an accurate approximation to predict the beam angle, radiation properties, as well as the FPA and PRS parameters for beam and null forming. The mathematical formulation does suffer from a few limitations that may compromise the accuracy such as mutual coupling between the radiating elements, non-linearities, and variations in direction-dependent finite PRS properties. The presented model has been verified with simulations on CST Studio at 8 and 8.5 GHz, which reveals a close correspondence to the simulated results. The developed methods exhibit high computational efficiency and a minimal number of mathematical operations to generate the E-field radiation pattern. This shows that the model can be easily used to predict an approximate relation among the FPA height, PRS phase profile, and the desired steering angle for any general Fabry-Perot Antenna.

REFERENCES

[1] Parker, D. and D. C. Zimmermann, "Phased arrays-part 1: Theory and architectures," *IEEE Transactions on Microwave Theory and Techniques*, Vol. 50, No. 3, 678–687, Mar. 2002.

[2] Ghasemi, A., S. N. Burokur, A. Dhouibi, and A. de Lustrac, "High beam steering in Fabry-Pérot leaky-wave antennas," *IEEE Antennas and Wireless Propagation Letters*, Vol. 12, 261–264, 2013.

[3] Ji, L.-Y., Y. J. Guo, P.-Y. Qin, S.-X. Gong, and R. Mittra, "A reconfigurable partially reflective surface (PRS) antenna for beam steering," *IEEE Transactions on Antennas and Propagation*, Vol. 63, No. 6, 2387–2395, Jun. 2015.

[4] Zhang, G., M. Su, Y. Zhang, A. Wang, and C. Pan, "Methodology and implementation of beam steering using C-shaped split rings for Fabry-Pérot antennas," *IEEE Transactions on Antennas and Propagation*, Vol. 71, No. 3, 2268–2277, Mar. 2023.

[5] Goudarzi, A., M. M. Honari, and R. Mirzavand, "A millimeter-wave Fabry-Pérot cavity antenna with unidirectional beam scanning capability for 5G applications," *IEEE Transactions on Antennas and Propagation*, Vol. 70, No. 3, 1787–1796, Mar. 2022.

[6] Xie, P., G. Wang, H. Li, and J. Liang, "A dual-polarized two-dimensional beam-steering Fabry-Pérot cavity antenna with a reconfigurable partially reflecting surface," *IEEE Antennas and Wireless Propagation Letters*, Vol. 16, 2370–2374, 2017.

[7] Reis, J. R., R. F. S. Caldeirinha, A. Hammoudeh, and N. Copner, "Electronically reconfigurable FSS-inspired transmitarray for 2-D beamsteering," *IEEE Transactions on Antennas and Propagation*, Vol. 65, No. 9, 4880–4885, Sep. 2017.

[8] Guzmán-Quirós, R., A. R. Weily, J. L. Gómez-Tornero, and Y. J. Guo, "A Fabry-Pérot antenna with two-dimensional electronic beam scanning," *IEEE Transactions on Antennas and Propagation*, Vol. 64, No. 4, 1536–1541, 2016.

[9] De Mello, R. G. L., A. C. Lepage, and X. Begaud, "Taming Fabry-Pérot resonances in a dual-metasurface multiband antenna with beam steering in one of the bands," *Scientific Reports*, Vol. 13, No. 1, 9871, 2023.

[10] Ourir, A., S. N. Burokur, R. Yahiaoui, and A. d. Lustrac, "Directive metamaterial-based subwavelength resonant cavity antennas — Applications for beam steering," *Comptes Rendus Physique*, Vol. 10, No. 5, 414–422, 2009.

[11] Afzal, M. U. and K. P. Esselle, "Steering the beam of medium-to-high gain antennas using near-field phase transformation," *IEEE Transactions on Antennas and Propagation*, Vol. 65, No. 4, 1680–1690, Apr. 2017.

[12] Yang, X., S. Xu, F. Yang, M. Li, Y. Hou, S. Jiang, and L. Liu, "A broadband high-efficiency reconfigurable reflectarray antenna using mechanically rotational elements," *IEEE Transactions on Antennas and Propagation*, Vol. 65, No. 8, 3959–3966, 2017.

[13] Hussain, M., K.-G. Lee, and D. Kim, "Tapered high-gain Fabry-Pérot cavity antenna with high sidelobe suppression for 5G industry," *Scientific Reports*, Vol. 13, No. 1, 15744, 2023.

[14] Hu, Y.-D., X.-H. Wang, S.-W. Qu, and B.-Z. Wang, "A wideband high-efficiency compact Fabry-Pérot resonant antenna with multilayer partially reflective surface," *IEEE Antennas and Wireless Propagation Letters*, Vol. 21, No. 10, 2100–2104, Oct. 2022.

[15] Liu, X., Z. Yan, E. Wang, T. Zhang, and F. Fan, "Magnetoelectric dipole-fed Fabry-Pérot antenna with wideband RCS reduction based on multilayer metasurface," *IEEE Antennas and Wireless Propagation Letters*, Vol. 20, No. 7, 1342–1346, Jul. 2021.

[16] Trentini, G. V., "Partially reflecting sheet arrays," *IRE Transactions on Antennas and Propagation*, Vol. 4, No. 4, 666–671, Oct. 1956.

[17] Liu, W. E. I., Z. N. Chen, and X. Qing, "Miniature wideband non-uniform metasurface antenna using equivalent circuit model," *IEEE Transactions on Antennas and Propagation*, Vol. 68, No. 7, 5652–5657, Jul. 2020.

[18] Zhao, T., D. R. Jackson, J. T. Williams, and A. A. Oliner, "General formulas for 2-D leaky-wave antennas," *IEEE Transactions on Antennas and Propagation*, Vol. 53, No. 11, 3525–3533, 2005.

[19] Boutayeb, H. and T. A. Denidni, "Internally excited Fabry-Pérot type cavity: Power normalization and directivity evaluation," *IEEE Antennas and Wireless Propagation Letters*, Vol. 5, 159–162, 2006.

[20] Zhou, L., X. Duan, Z. Luo, Y. Zhou, and X. Chen, "High directivity Fabry-Pérot antenna with a nonuniform partially reflective surface and a phase correcting structure," *IEEE Transactions on Antennas and Propagation*, Vol. 68, No. 11, 7601–7606, Nov. 2020.

[21] Sengupta, S., D. R. Jackson, and S. A. Long, "Modal analysis and propagation characteristics of leaky waves on a 2-D periodic leaky-wave antenna," *IEEE Transactions on Microwave Theory and Techniques*, Vol. 66, No. 3, 1181–1191, Mar. 2018.

[22] Ran, X., X.-H. Wang, Y.-D. Hu, S.-W. Qu, and B.-Z. Wang, "Dual-polarized nonuniform Fabry-Pérot cavity antenna with flat-topped radiation pattern," *IEEE Antennas and Wireless Propagation Letters*, Vol. 21, No. 5, 1060–1064, May 2022.

[23] Liang, Q., B. K. Lau, and G. Zhou, "Beam-reconfigurable antenna with inductive partially reflective surface and parasitic elements," TechRxiv, Mar. 2023.